Proton-^{90}Zr interaction at sub-Coulomb proton energies

C. E. Laird

Eastern Kentucky University, Richmond, Kentucky

David Flynn,* Robert L. Hershberger,* and Fletcher Gabbard

University of Kentucky, Lexington, Kentucky

(Received 10 November 1986)

The proton-^{90}Zr interaction at sub-Coulomb energies has been investigated in the context of the Lane model, with isospin coupling included, and with alternate decay modes represented with the Hauser-Feshbach model. Scattering and reaction cross sections were accurately measured in order to obtain enough information to constrain the real and absorptive parts of the proton potential. Differential elastic scattering excitation functions were measured at back angles of 135° and 165° from 2 to 7 MeV, with cross section accuracies of 3%. The energy range was sufficient to go from a region where the backscattering was predominantly Coulomb, enabling additional checks on the cross section accuracies, to a region where the gross structure of the cross sections deviated significantly from Rutherford scattering. Radiative capture cross sections were measured from 1.9 to 5.7 MeV proton energies. The capture cross sections were obtained by summing the measured cross sections for the first two primary gamma rays in addition to some 34 other transitions which terminated on the ground and first excited state. The total inelastic scattering cross section to all ^{90}Zr excited states (except the first excited state which has been previously measured) was measured at several energies between 3.9 and 5.7 MeV by observing the radiative decay of the residual, excited ^{90}Zr nuclei. The analysis yielded several model parameters suggestive of large nuclear structure effects. The depth of the absorptive potential was found to vary as $W_D = 2.73 + 0.70\, E_p$ in the 2 to 7 MeV proton energy range studied. A real diffuseness of 0.54 fm, significantly smaller than that obtained in neighboring nuclei, was obtained.

I. INTRODUCTION

Precision measurements of total (p,n) cross sections at sub-Coulomb proton energies have proven to be a valuable aid to understanding properties of proton-nucleus interactions at low bombarding energies, because they frequently represent almost the entire absorptive cross sections. The first clear observation of a single-particle or potential resonance (SPR) in an excitation function for a medium- or heavy-mass nucleus was made in very accurate measurements of total (p,n) cross sections for isotopes of tin.[1] Subsequent studies of (p,n) and (p,p) cross sections in the mass-100 region have been used to study the systematic variation with atomic-mass number of the proton absorption throughout the region.[2-7]

In this mass region the compound nucleus, formed by protons with energies below the Coulomb barrier, finds neutron decay, when energetically possible, the dominant decay mode. Below the (p,n) threshold, other reaction channels, principally (p,p), (p,p'), and (p,γ), account for the major part of the proton absorption cross section. An objective of the present work was to extend the study of the sub-Coulomb proton absorption of nuclei in the mass-100 region by measuring (p,p), (p,p'), and (p,γ) cross sections when the (p,n) channel is closed. ^{90}Zr with a (p,n) threshold at 6.97 MeV was chosen for study in the energy range of $E_p = 1.9$ to 7.0 MeV. In this mass region, the (p,γ) cross sections dominate below a proton energy of 2.5 MeV, but diminish in importance at higher energies as

(p,p) and (p,p') cross sections become larger.

For proton energies below the Coulomb barrier,[2-7] studies of absorbing properties of nuclei in this mass range showed that, near mass 90, when the target nucleus is represented by a spherical optical potential, the absorptive potential is unusually small compared to global values of this parameter. Similarly small absorptive potentials have been observed in neutron elastic scattering in this mass region.[8] Also, the measurements of elastic scattering from ^{92}Zr performed by Schrils et al.[4] could not be fitted unless the real potential diffuseness (or radius) was decreased some 15% from global values. It is expected that the small absorptive potential and the small real diffuseness are shell effects.[2-5] The major neutron shell closure at $N = 50$ and the proton subshell closure at $Z = 40$ make ^{90}Zr an especially interesting target for study.

Details of the experimental methods are presented in Sec. II. The data reduction and experimental results are presented in Sec. III. Section IV contains a description of the nuclear models and of the model parameters used in the analysis of the experimental data. Section V contains a discussion of the results.

II. EXPERIMENTAL PROCEDURES

Measurements of (p,p), (p,p'γ), and (p,γ) cross sections on targets of ^{90}Zr were obtained using the University of Kentucky 6.5 MeV HVEC Van de Graaff accelerator and associated facilities. Gamma-ray spectra were measured

with a 131 cm^3 or an 80 cm^3 Ge(Li) detector for proton energies from 1.9 to 5.7 MeV. No (p,γ) measurements were made above 5.7 MeV because the high yield of fast neutrons is a hazard to the life of the Ge(Li) detectors. Proton elastic-scattering differential cross sections were measured in the energy range from 2 to 7 MeV in a scattering chamber with two surface barrier detectors located at 135° and 165° from the beam direction and subtending solid angles of 0.371±0.003 msr. Pulses from the detectors were amplified and those corresponding to elastically scattered protons were selected with single-channel analyzers and scaled. Further details of the experimental techniques used in the scattering measurements are described in Refs. 4 and 7.

Inelastic scattering was not measured with the scattering chamber because inelastic protons could not be adequately resolved from those scattered by target impurities and contaminants. Inelastic scattering cross sections were obtained from the γ-ray spectra using γ rays emitted from known states in ^{90}Zr.

The target foils were made by rolling zirconium metal enriched to 97.6% in ^{90}Zr. The target thicknesses and uniformity were determined from the elastic proton scattering at energies of 2 MeV where the scattering is predominantly Coulomb. The thicknesses were checked by accurately measuring the weight and area of the target foils, and the two methods agreed to within 2%. The resulting thicknesses of the two targets used in the experiments were 439±9 and 885±53 μg/cm^2. Impurities in the targets were determined, by chemical analysis and by γ-ray counting, to be less than 1% for both targets.

For γ-ray measurements, the targets were mounted in a glass chamber and electrically connected to the Faraday cup and beam stop. The targets were biased at +300 V to suppress secondary electron emission. The system was evacuated to 5×10^{-6} Torr using, in addition to conventional diffusion pumps, an in-line liquid-nitrogen cold trap which was used to cryogenically pump the system to reduce the deposition of contaminants onto the target.

Aluminum γ-ray absorbers with a total thickness of 1.34 g/cm^2 were placed between the target and the detector to prevent pulse summing and to reduce low-energy signals which degrade the resolution of the detector. In addition, the beam current was kept below 2 μA to hold the dead time below 13% and maintain good resolution in the detector.

The effective dead time of the system was determined by introducing a signal from a pulser into the input of the detector preamplifier so that the pulses were accumulated into each γ-ray spectrum. A check of the dead time was made by gating a clock with the busy signal from the analog-to-digital converter (ADC). The corrected yields differed by less than 2% after using both methods.

The Ge(Li) detector was located at an angle of 125° to the beam direction and at a distance of approximately 7 cm from the target. The angle of 125°, a zero of $P_2(\cos\theta)$, made it possible to deduce the total cross section from the measured differential cross section, assuming that terms of order higher than P_2 were small. The efficiencies of the Ge(Li) detectors were measured from 0.088 to 3.0 MeV using a National Bureau of Standards (NBS) cali-

brated mixed gamma source, a NBS calibrated ^{152}Eu source, and a ^{56}Co source,[9] and from 1.5 to 11.542 MeV using the ^{27}Al(p,γ)^{28}Si resonances at E_p=0.992 and 1.800 MeV and the known relative γ-ray intensities.[10] To check the accuracy of the capture cross-section measurements, the absolute strength of the 0.992 MeV resonance in ^{27}Al(p,γ)^{28}Si was measured and found to be in good agreement with values recently measured by Antilla et al.[10] Also, the absolute and relative yields for five γ rays from 0.846 to 2.836 MeV produced by the stopping of 2 MeV protons in an infinitely thick, pure (99.99%) aluminum target agreed within 6% to values measured by Kenny.[11]

III. DATA REDUCTION

A. ^{90}Zr(p,p)

Differential cross sections were obtained for protons elastically scattered from ^{90}Zr at 135° and 165° for 45 proton energies from 2 to 7 MeV. In order to determine the optical model parameters in the analysis described in Sec. IV, it was necessary to measure the proton excitation function with a precision of better than 2%. This necessitated the use of the thinner (439 μg/cm^2) target since it was the more uniform. Corrections were made for dead time in the electronics and for proton energy loss in the target in the manner described in Ref. 4. The corrected yields were normalized to the Rutherford cross section at 2.0 MeV. Figure 1 shows these corrected yields, plotted as ratio to Rutherford (the solid circles), as a function of proton energy. The precision of the yields is better than 2% and the absolute accuracy of the cross sections tabu-
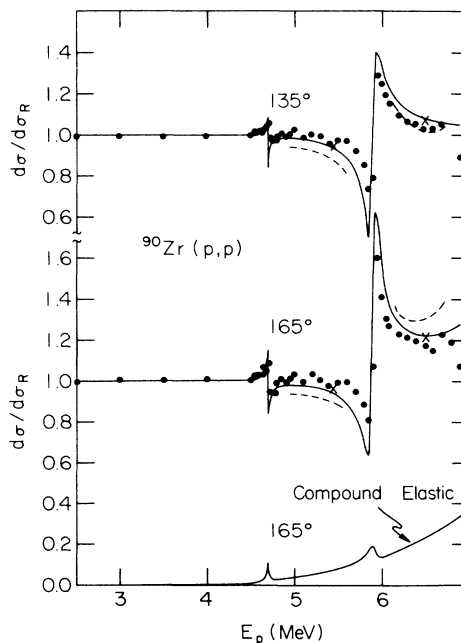

FIG. 1. Relative proton differential cross sections including compound elastic scattering. The solid curves are the fits obtained in the analysis. The dashed lines were calculated using global parameters. The crosses are discussed in the text.

lated in Ref. 12 is estimated to be 3%. A detailed summary of the uncertainties is given in Table II of Ref. 7. The dashed lines are from model calculations done with global parameters while the solid lines are the resultant fit to the data. This and the remainder of the figure will be discussed in Sec. IV A.

B. ⁹⁰Zr(p,p'γ)

The inelastic scattering cross sections can be measured, in principle, by observing the γ rays emitted from the target nucleus. Since the barrier penetrability (both in the incoming and outgoing channels) of the protons is highly energy and angular momentum dependent, the outgoing protons tend to leave the target nucleus in low-energy states having small energy and angular-momentum differences from the ground state. In the case of the spin-zero target ⁹⁰Zr, the inelastic scattering of protons leads to the population of a few discrete excited states in ⁹⁰Zr. According to the known decay scheme,[9] only the first, second, third, and fifth levels decay directly to the ground state while the other states cascade through these four levels. Thus, by measuring the γ decay of these four states the total (p,p'γ) cross section could be obtained.

However, the first excited state decays by an $E0$ internal conversion or pair process and could not be studied through observation of gamma rays. The total (p,p') cross section to all excited states except the first was obtained by measuring γ rays corresponding to the decay of the second (2186 keV), third (2319 keV), and fifth (2748 keV) excited states. The fifth-excited-state decay to the ground state was deduced from the 96% branch to the third excited state which gives a 562 keV γ ray.[9] This contribution to the total cross section was never more than about two percent. The first excited state, whose decay was not measured, is fed by the 2186 keV second excited state, as well as being populated directly by the outgoing protons. Since the 2186 keV level has only a 0.03% branching ratio to the first excited state, the unmeasured cascade which passed through the first excited state was neglected.

The γ-ray spectra occurring from proton reactions on ⁹⁰Zr were analyzed with the program SAMPO (Ref. 13) using the IBM 3081 computer at the University of Kentucky Computing Center. This program automatically identified peaks in the spectra, integrated the peaks after subtracting an appropriate background, and computed the energies for each peak. The peaks were identified by comparison with known decay and energy-level schemes.[9,14,15]

Cross sections for ⁹⁰Zr(p,p'γ) shown in Fig. 2 and listed in Table I, were obtained at 12 different proton energies ranging from 4.2 to 5.7 MeV. The proton energies listed in Table I are mean energies, computed from the incident proton energies, target fitness, and target stopping power. The values plotted in Fig. 2 are reduced cross sections or strength functions (SF) generally defined by

$$[\sigma] = R\sigma(p,X) \Big/ \left[4\pi^2 k^{-2} \sum_l (2l+1)P_l \right],$$

where k is the wave number for the incident proton, P_l is the Coulomb penetrability factor for l-wave protons evaluated at a radius of $R = 1.45A^{1/3}$ fm, and X refers to
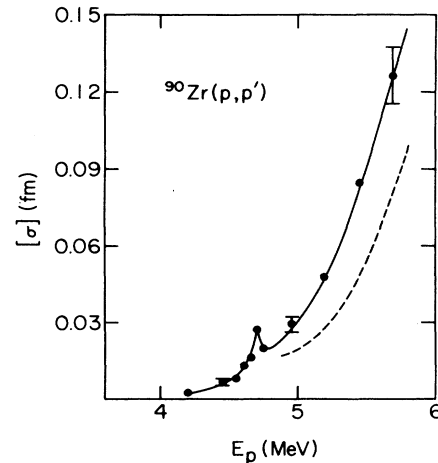

FIG. 2. Inelastic reduced cross sections to energy levels above the first excited state. The dots represent experimental data. The solid line represents the results of the model fit using $a_R = 0.73$ fm, $W_D = 18$ MeV. The dashed line was obtained using $a_R = 0.53$ fm, $W_D = 6$ MeV. The error bars represent a 5% statistical error.

the particle emitted in the reactions $(X=p',\gamma,$ n, γ, etc.). The structure in the excitation function near 4.7 MeV is the $\frac{5}{2}^+$ isobaric analog resonance (IAR). The error bar shown represents an estimated standard deviation of 5% obtained from counting statistics only. Including uncertainties in detector efficiency (3—5 % for γ-ray energies below 4.2 MeV to 13% for energies above 10 MeV), target thickness (2% and 6%), and other smaller effects gives an estimated overall accuracy in the cross sections of 10%. In the analysis of Sec. IV, the (p,p') cross sections to the first-excited state were included using the report of Moore et al.[16] who observed the inelastic protons to measure the inelastic cross sections for incident energies near and above 5.7 MeV.

C. ⁹⁰Zr(p,γ)⁹¹Nb

Accurate measurements of total ⁹⁰Zr(p,γ) cross sections are complicated by the multiplicity of γ rays emitted in

TABLE I. Total ⁹⁰Zr(p,p') cross sections to energy levels above the first-excited state.

E_p (MeV)	$\sigma(p,p')$ (mb)
4.206	0.0149
4.454	0.0658
4.554	0.089
4.604	0.155
4.663	0.209
4.703	0.369
4.753	0.287
4.951	0.539
5.199	1.18
5.448	2.70
5.696	5.07

TABLE II. Measured cross sections of eight lowest-energy γ rays to the ground state or first-excited state.

E_p (MeV)	E_γ (keV)								$\sum_{j=1}^{8} \sigma$ (μb)
	1082	1208	1508	1581	1637	1740	1790	1963	
	σ (μb) ($\pm 10\%$)								
1.973	0.8	2.5	0.6	0.4	0	0.2	0	0.4	4.9
2.247	4.7	8.3	3.2	1.5	0.4	0.5	0.3	1.0	2.0
2.472	16.3	16.8	10.1	4.9	1.1	2.2	0.9	3.5	55.8
2.671	16.1	26.1	11.5	4.7	2.3	2.4	1.3	4.0	68.3
2.96	44.7	45.9	28.1	14.0	4.4	7.8	4.1	11.6	161
3.092	47.5	60.8	33.2	17.4	5.5	8.3	6.8	13.3	193
3.206	52.6	57.0	28.5	18.8	7.1	10.4	12.9	17.4	205
3.474	144	104	50.9	39.8	19.6	16.1	12.3	28.7	415
3.708	197	181	72.5	76.4	28.9	24.4	21.9	46.6	648
3.974	261	215	106	113	46.8	37.7	39.5	55.2	873
3.985	282	224	105	104	44.8	36.8	38.0	56.9	892
4.205	363	305	153	173	82.0	66.6	69.8	93.5	1310
4.454	508	415	207	249	116	94.1	106	146	1840
4.553	572	472	231	285	127	98.2	161	152	2100
4.603	647	516	255	327	146	106	151	193	2340
4.663	947	650	301	401	176	167	350	310	3300
4.702	980	692	347	461	206	168	324	226	3400
4.752	747	599	288	389	178	131	161	221	2720
4.951	781	638	291	419	194	119	171	245	2860
5.199	1040	764	393	548	241	151	232	291	3660
5.447	1230	1030	477	742	340	194	301	379	4690
5.695	1450	1150	497	832	393	202	365	421	5300

the decay of a highly excited nucleus. However, the cross sections can be determined by combining partial cross sections from the following transitions: (1) those primary γ rays which connect the capturing states directly to the ground or first excited states, and (2) secondary transitions from excited states below 4.2 MeV excitation energy which result from unmeasured primaries and go directly to the ground or to the first excited state. These two sets of transitions will account for all primary transitions except those which cascade through levels above 4.2 MeV to the two lowest levels, by-passing the measured secondaries. The correction for this by-pass cascade is small, and can be estimated by extrapolation from observed transition strengths using the Brink-Axel hypothesis (Ref. 17 and references therein) to model the energy dependence of γ-ray transition strength, as described below.

Thirty-four low energy γ-ray transitions were identified in ^{91}Nb. All of these transitions had been previously reported by Rauch.[15] Each of these corresponded to a transition which started at a level of excitation energy of less than 4.2 MeV and terminated in the ground state or the 105 keV first-excited state. Primary γ rays corresponding

TABLE III. Cross sections of selected γ rays to the ground state or first-excited state.

E_p (MeV)	σ_{2-4}[a] (μb)	σ_{un}[b] (μb)	σ_1[c] (μb)	σ_0[d] (μb)	σ_T[e] (μb)
2.247	2.16	1.40	3.31	1.29	28.2
2.472	7.3	4.65	15.00	1.73	84.5
2.960	2.1	21.7	46.1	5.38	256
3.474	57.4	62.0	50.2	17.6	602
3.974	106	155	81.7	50.2	1270
4.951	240	667	97.3	82.7	3950
5.695	1020	1340	151	7.4	7930

[a]σ_{2-4} is the cross section for all γ rays of energies between 1.963 and 4.2 MeV.

[b]σ_{un} is an estimate of the cross section of the unobserved γ rays terminating on the ground or first excited state. These γ rays have energies greater than 4.2 MeV and less than the energy of the primary γ ray to the first excited state.

[c]σ_1 is the cross section of the primary γ rays to the excited state.

[d]σ_0 is the cross section of the primary γ rays to the ground state.

[e]σ_T is the total cross section for producing γ rays which leave the nucleus in the ground or first excited state. This result is obtained by summing the various cross sections listed in the second, third, fourth, and fifth columns with the last column of Table II.

to transitions directly from the capturing state to the ground and first excited states were also observed. Gamma-ray yields from these 36 transitions were measured at seven incident proton energies from 2 to 5.7 MeV, and corresponding cross sections were deduced.

Since the largest contribution to the cross section came from the eight lowest-energy γ-ray transitions, further measurements of these eight were performed, at 15 additional proton energies from 1.9 to 5.7 MeV. Cross sections for each of these eight transitions were obtained for 22 incident proton energies, and the results are listed in Table II. The number at the top of each of the eight columns is the energy of the γ ray measured. For each proton energy, the eight cross sections are summed to give the result in the right-most column. The underlined energies are those at which 36 gamma transitions were measured. Table III contains the results above 2 MeV and the total deduced (p,γ) cross sections. Figure 3 shows these data as reduced cross section defined as in Eq. (1). Figure 4 shows the cross section (rather than the reduced cross section for the sake of clarity) for the primary transition to the first excited state and will be discussed in Sec. IV C.

In Fig. 3, the solid circles, defined for σ(p,γ) as in Eq. (1), show the total (p,γ) cross section as a function of mean proton energy derived from the sum of the partial cross sections as labeled in the figure and discussed below. The total reduced cross section is the sum of the contributions from the eight low-energy γ rays, the γ rays from 2 to 4 MeV, the two primary γ rays, and the unobserved γ rays above 4 MeV. The estimate of the reduced cross sections of γ rays with energies too high to be identified (>4.2 MeV) is shown as the lower dotted line. This esti-
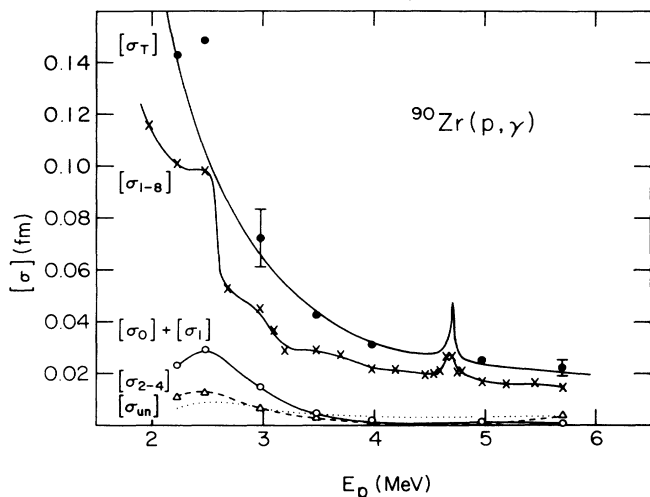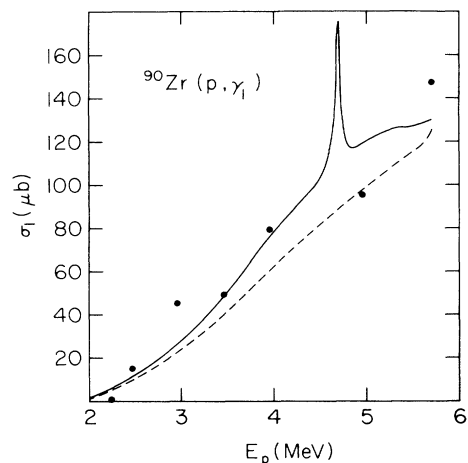

FIG. 4. Cross sections for the primary gamma-ray transition to the first excited state. The solid line represents the results of the model fit. The dashed line represents the fit using the standard dipole gamma-ray strength function.

mate was obtained by performing Hauser-Feshbach calculations at various incident proton energies to predict first the probability that the initial compound nuclear state deexcited to an energy region ($E > 4.2$ MeV) of width ΔE (typically 500 keV), and second, the probability that this excited region would decay to the ground state or first excited state. These probabilities were combined to predict the probability that the excited compound nucleus decayed into an excited state and, subsequently, to the unobserved ground or first excited states without cascading through the observed levels below 4.2 MeV. This one-step, by-pass cascade was deemed sufficient because first order estimates were typically 10% and a two-stop by-pass cascade would be far smaller than 10% of the one-step by-pass cascade, since at lower excitation energies a larger fraction of the cascade falls below 4.2 MeV. Subsequent calculations using the computer code GNASH (Ref. 18) confirmed this prediction. The standard deviation associated with the total (p,γ) cross sections is estimated to be 15%. This estimate takes into account previously stated uncertainties (see Sec. III B) as well as the uncertainties in the estimated unmeasured γ rays with energies greater than 4.2 MeV (2%) and in the correction for the 0.96% ^{91}Zr present in the target. Since ^{91}Zr(p,nγ)^{91}Nb produces the same low-energy γ rays as does ^{90}Zr(p,γ), the correction to the γ-ray yields introduced an additional uncertainty of up to 7%.

FIG. 3. Reduced (p,γ) cross sections. The crosses represent the sum of eight gamma transitions from the low-lying excited states. The circles are the contribution from primary gamma transitions to the ground and metastable states. The triangles are due to nuclear levels from 2 to 4 MeV. The dotted line represents transitions from levels above 4 MeV which were unobservable. The solid circles are the total reduced cross section. The lines are to show the trend of the data, except that the uppermost curve is the total reduced (p,γ) cross section computed with the model.

IV. ANALYSIS

In the analysis of the ^{90}Zr plus proton reaction data, it was assumed that the reaction cross sections at these low energies are described by the Hauser-Feshbach model,[19] using the Lane model[20] as described in the Appendix to calculate the transmission coefficients for absorption and compound elastic scattering of protons. The Lane model provides for isobaric analog resonances by coupling the proton plus target state to the bound neutron plus analog state. Other particle transmission coefficients from the compound nucleus were determined by a conventional op-
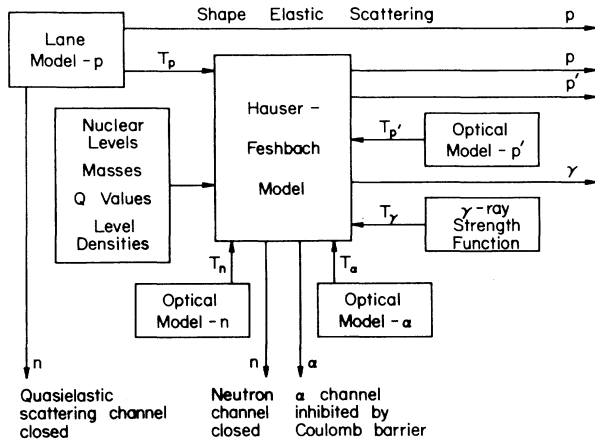
FIG. 5. Interrelation among various nuclear models.

tical model. Radiative decay probabilities were determined by a γ-ray strength function which initially was assumed to be given by the tail of the giant dipole resonance.[17] Figure 5 shows the relationship among the various models and assumptions used in this analysis.

Masses and Q values were taken from Wapstra and Bos.[21] Energies, spins, and parities of low-lying states in the various nuclides were taken from Lederer and Shirley.[9] For higher excitation energies, level densities were computed with the backshifted Fermi-gas model.[22] The level-density parameter a was taken from the results of Dilg et al.[22] The energy shift parameter Δ was obtained in the manner suggested by Johnson:[17] Δ was adjusted until the calculated level density was equal to the level density obtained from counting discrete states in the nuclide of interest, at excitation energies as high as possible, but low enough so that few states were missed. Width fluctuation corrections to the Hauser-Feshbach model were obtained from the Lane-Dresner formalism.[23]

A. Proton elastic potential

The Lane model was used to represent the proton-nucleus interaction in the present analysis to reproduce the detailed shape of the cross sections near the IAR's and to enable the determination of the potential depths for $l=0$ and $l=2$. The use of this model gives potential parameters which are negligibly different from the standard optical model.[4,6] The radii were assumed to be given by $r_R = 1.20$ fm, $r_{so} = 1.03$ fm, and $r_D = 1.30$ fm. The diffuseness were assumed to be $a_{so} = 0.60$ fm and $a_D = 0.40$ fm, while that for the real potential, a_R, was obtained by fitting the cross sections. The Coulomb energy, Δ_C, was taken to be 11.868 MeV, as reported by Courtney and Fox.[24] The well depth V is given by Eq. (A8) in the Appendix. The energy dependence β is assumed to 0.32.[25] The Coulomb correction V_C is assumed to be $0.45Z/A^{1/3}$. V_1 is the depth of the real part of the asymmetry potential defined in the Appendix, which is $\text{Re}(v_1) = 4V_1 f(x_R)$. It has been shown[26] that a value of $V_1 = 31.4 \pm 2.0$ MeV is required to provide the observed splitting between the $3s_{1/2}$ IAR and the $3s_{1/2}$ SPR.

Having fixed the real potential radius and using the l-dependent potential procedure suggested by Schrils,[4] V_0 and V_{so} were determined by fitting the observed $\frac{5}{2}^+$ and $\frac{1}{2}^+$ resonances and centroid of the $\frac{3}{2}^+$ resonance. Fitting to the first two resonances is critical to obtaining a_R and W_D in subsequent analysis in the 4.5—5.5 MeV range. In order to correctly locate the $3s_{1/2}$ SPR, V_1 was set to 29.7 MeV—a value consistent with the previously stated range.[25,26] The "centroid" energies were computed using spectroscopic factors to weight the observed resonance positions, found in $^{90}\text{Zr}(^3\text{He,d})$ measurements[27,28] and in ^{90}Zr (d,p) measurements.[14] Parameters of the IAR's are given in Table IV.

The resulting potential parameters are listed in Table V. The resulting values of V_0 are consistent with those observed by Johnson[2] for this mass range; and the resulting V_0 $(l=0)$ was about 1 MeV higher than V_0 $(l=2)$, which was the same difference observed in both ^{92}Zr and ^{94}Zr by Schrills et al.[4] The spin orbit potential obtained in the present work is within 5% of the 6.4 MeV value previously adopted in this mass-energy range.[2–4]

Schrils et al.[4] used proton elastic scattering at energies above 4 MeV to study the real potential geometry for ^{92}Zr. These authors determined the value of a_R by fixing r_R and varying a_R to fit the 135° and 165° elastic scattering cross sections which fell significantly below the Rutherford values toward high energy. We followed this procedure.

Below the (p,n) threshold compound elastic scattering contributes significantly to the total elastic cross section. This can be seen in the two smooth curves for 165° in Fig. 1. The lower curve gives the calculated contribution from compound elastic scattering at 165° and the smooth the center of this graph gives the total elastic scattering (including compound) cross sections normalized to Rutherford scattering. Thus, a fit to the data must account both for scattering at the nuclear surface, strongly dependent on a_R, and for compound elastic scattering, strongly dependent on W_D.

Although the Lane model used allows for the placement of IAR's at the proper energy, it does not account for the configuration mixing in the parent nucleus, or the associated spectroscopic factors.[29] To compensate for this omission the cross sections to be fitted were increased by 4% near 5.5 MeV and lowered by 4% near 6.5 MeV (shown by the ×'s in Fig. 1). This estimate was based on a spectroscopic factor of 0.66 for the $S_{1/2}$ resonance.[14] Calculations with and without the isospin coupling included showed that the model overestimates the total elas-

TABLE IV. Parameters of the IAR's

Resonance	Energy[a] primary fragment (MeV)	Spectroscopic[a] factor (d,p)	Centroid[a] energy (MeV)
$d_{5/2}$	4.71	0.75	4.75
$S_{1/2}$	5.92	0.66	6.28
$d_{3/2}$	6.80	0.56	7.33

[a]Reference 14.
[b]Reference 26.

TABLE V. Optical model parameters deduced from the data analysis.

Channel	V_0 $(l \neq 2)$	V_0 $(l = 2)$	V_{so}	V_1	a_R	W_0	dW_D/dE
Incident (p)	55.6[a]	54.2	6.1	29.7	0.54	2.63	0.73
Outgoing (p')	55.6	54.2	0.0	29.7	0.73	18.0	0

$$W_D = W_0 + (dW_D/dE)E_p$$

[a]Fitting the S wave centroid instead of the fragment would yield $V_0 = 55.2$ MeV.

tic scattering effects by 35% or 4% of Rutherford. Using these modified data a χ^2 analysis was performed with the results plotted in Fig. 6 as a function of W_D for various values of a_R. All of the values of a_R less than 0.62 fm give adequate fits. Values adopted in the present work were $a_R = 0.54 \pm 0.04$ fm and $W_D = 7.0 \pm 1.0$ MeV at 6 MeV proton energy.

To complete the specification of the proton potential in the 2—7 MeV energy range it is noted that the absorptive potential may be energy dependent.[5,30] The results obtained above indicate only that the proton absorptive potential between 5 and 7 MeV (the range of the useful scattering data) is ~ 7 MeV. It is expected from systematic analyses of zirconium and molybdenum (p,n) strength functions[5] that the absorptive potential becomes significantly smaller at lower proton energies. By comparing fragments of the $3s$ SPR around $E_p = 0.66$ MeV with model calculations, the depth of the absorptive potential has been estimated to be ~ 3 MeV at that energy.[26] In the analysis of the (p,γ) and (p,p') data to be discussed in Sec. III B, $W_D = 2.73 + 0.70 E_p$ was taken as the absorptive potential consistent with the above results.

Shown in Fig. 7 are the volume integrals of the absorptive potential well depths obtained for other nuclei in this mass region by Johnson et al.[2] and Flynn et al.[3] The solid triangle at $A = 90$ corresponds to the present result at 3 MeV proton energy and the solid square to 6 MeV. The present result is consistent with the previously reported trend of the absorptive potentials for this mass region.

The absorptive strength, extrapolated to 12.5 MeV, yields a volume integral per nucleon of ~ 91 MeV fm^3. Thus, the present energy dependent absorptive potential is
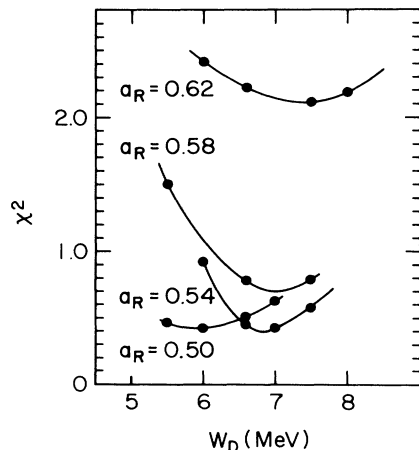
consistent with the value of 98 MeV fm^3 obtained by Schulte et al.[31]

B. Inelastic proton potential

The important open channels in the compound-nucleus decay of ^{91}Nb were the compound elastic scattering, inelastic proton scattering, and proton capture. The inelastic proton potential model differed from the elastic potential in two respects; the inelastic channels did not include a spin-orbit term and the values of the parameters a_R and W_D were larger than in the potential used in the elastic scattering analysis. The Hauser-Fesbach code, HELGA,[7] was used to represent the compound-nucleus decay.

Traditionally, the potential representing the nucleon-nucleus interaction is assumed to be independent of the state of excitation of the nucleus. If this were true, then the results of the analysis would have yielded an inelastic proton potential which was the same as the elastic proton potential. The fit to the inelastic data is illustrated in Fig. 2. The dashed line was calculated from the model using the same potential as was used in the elastic scattering. The solid line shows the fit with $a_R = 0.73$ fm and $W_D = 18$ to be consistent with global analysis.[25,32] Com-
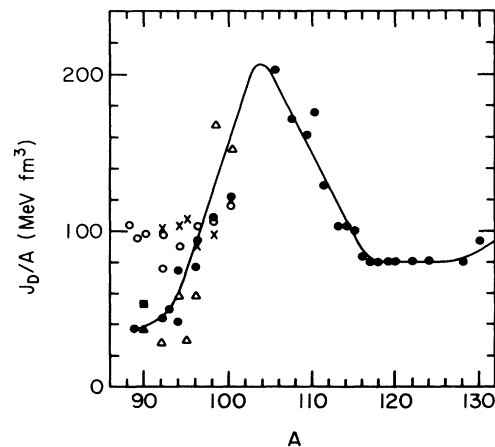
FIG. 7. Volume integral per nucleon of the absorptive potential for mass-100 nuclides. The solid triangle and the solid square are the values deduced in this study for proton energies of 3 MeV and 6 MeV, respectively. The crosses and the triangles are the results from Ref. 5 for the same respective energies. The solid circles represent the results of previous optical model analyses of (p,n) cross sections (Refs. 1, 3, 6, and 7). The open circles represent the results of optical-model analysis (Refs. 31 and 43) of proton scattering measurements for proton energies which are above the Coulomb barrier (8—15 MeV).

FIG. 6. Chi-square versus absorptive potential for several real diffuseness.

pared to these values the parameters a_R and W_D, which give fits to the elastic scattering data, are smaller.

Moore et al.[16] measured ^{90}Zr(p,p') cross sections to the first excited state. This was not measured in the present experiment. To further test the model with the larger values obtained for a_R and W_D, the ^{90}Zr(p,p') cross sections to the first excited state were calculated for proton energies between 5 and 6 MeV and were found to agree within 10% with the experimental results of Moore.

C. Gamma-ray strength function

Having constrained the elastic and inelastic proton potentials as discussed in the preceding sections, it is now possible to carefully examine the (p,γ) cross sections and extract information about the radiative decay of the compound nucleus. Transmission coefficients corresponding to decay of the ^{91}Nb compound nucleus by $E1$ radiation were obtained for use in the Hauser-Feshbach model from the expression

$$T_{E1} = 2\pi E_\gamma^3 S_{E1}(E_\gamma) ,$$

where E_γ is the energy of the dipole radiation and $S_{E1}(E_\gamma)$ is the $E1$ strength function.[17,33] Transmission coefficients for $M1$ radiation were assumed to be 14% of T_{E1} as suggested by Johnson.[2]

The dashed line shown in Fig. 8 is the $E1$ strength function extrapolated from the giant dipole resonance, using the parameters suggested by Johnson.[2] This strength function, in conjunction with the previously obtained elastic and inelastic potentials, was used to calculate total (p,γ) cross sections and proton radiative capture to the first excited state. The results of the calculation for (p,γ) are represented by the dashed line in Fig. 4. The final $E1$ strength function was determined by varying the three parameters in the dipole-resonance formulation of the strength function (centroid, width, maximum) to optimize the fit to the capture to the first excited state and the total capture cross sections while maintaining fits to the elastic

FIG. 8. Gamma-ray strength function. The dashed line is the function used in Ref. 17. The solid curve is the function deduced from this study.

and inelastic cross sections. This strength function is shown by the solid curve in Fig. 8. The final (p,γ_1) cross section is the solid curve in Fig. 4.

V. DISCUSSION OF RESULTS

Lane model analysis of the elastic scattering data has shown that both the diffuseness (<0.58 fm) and the absorptive potential (~ 7 MeV) are considerably lower than global optical model parameters. The small value for the diffuseness follows the trend observed[5] in ^{92}Zr and ^{94}Zr. It also compares favorably with those obtained in charge (i.e., proton), neutron, and matter distribution studies.[33−36] Greenlees et al.[34] analyzed proton elastic scattering data to obtain a matter distribution for ^{90}Zr characterized by a radius parameter 1.2 fm and a diffuseness of 0.57 fm. In addition, phenomenological and Hartree-Fock densities referred to in Barrett and Jackson[35] are consistent with a radius parameter of 1.1 fm and a diffuseness of 0.55 fm. All of these results indicate that the real diffuseness of ^{90}Zr is significantly smaller than those obtained from global parameter studies at higher proton energies.

The strength of the absorptive potential, W_D, has been determined to follow the trend previously observed for sub-Coulomb reactions. This trend toward smaller values of W_D near the closed shell model at $Z = 40$ and $N = 50$ agrees with the calculation of Grimes[30] indicating that shell-model and collective effects contribute to the anomalous behavior in the absorptive potential. The need to use different values for a_R and W_D in proton inelastic scattering appears to be due to a difference in nuclear structure between the ground and excited states of ^{90}Zr. In the light of the systematic behavior in W_D and a_R as the closed shell at $A = 90$ is approached, it is not unexpected that the promotion of particles out of the closed shell to form excited states of ^{90}Zr should decrease the effects of shell closure and hence tend to increase W_D and a_R.

The gamma-ray strength function found in this work shows a small deviation from the normally assumed Lorentzian tail. This deviation should not be surprising for the mass 90 region. Photonuclear reaction studies by many authors[37−42] on targets such as ^{88}Sr, ^{89}Y, ^{90}Zr, ^{93}Nb, and ^{92}Mo have shown significant non-Lorentzian structure well above the particle emission thresholds near 8−10 MeV. At lower energies, Obst et al.[41] observed considerable structure in (p,γ_0) reactions on ^{89}Y from about 10.5 MeV excitation energy up to and above the effective neutron emission threshold. Other authors[42] studying the gamma-ray strength function near mass 60 have found considerable deviation from the Lorentzian shape.

The large cross section found for radiative capture to the ground state is difficult to explain. The ground state of ^{91}Nb is $\frac{9}{2}^+$ ($g_{9/2}$), and $E1$ gamma transitions connect this state to $f_{7/2}$, $h_{9/2}$, and $h_{11/2}$ states; $M1$ transitions connect this state to $g_{7/2}$ and $g_{9/2}$ states. The model calculations indicate that the proton population of f, g, h, and i states are relatively low at these excitation energies. Weisskoff estimates of higher order gamma transition multipolarities, not included in this model calculation,
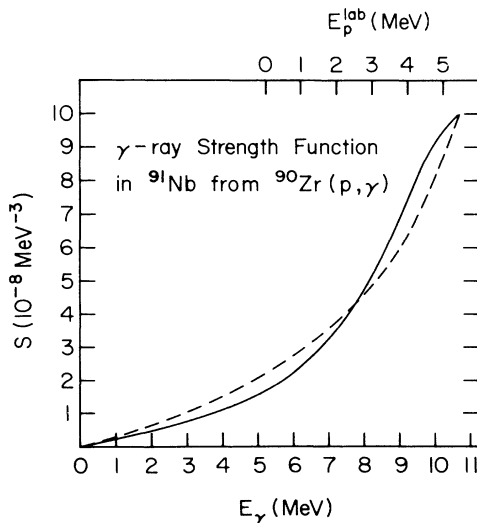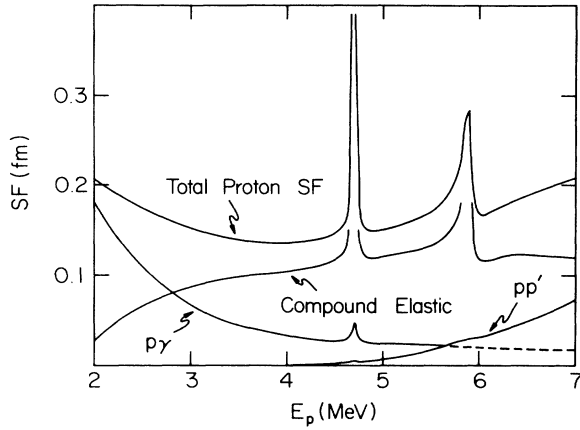
FIG. 9. Proton-^{90}Zr strength function. The total proton strength deduced in this study is shown with the contribution from each channel.

give transition probabilities several orders of magnitude lower than dipole transitions. These predictions of capture to the high-spin ground state are much smaller than observed. Enhancement of $E1$ radiation, or higher multipolarities by collective effects or other reaction mechanisms, could account for this discrepancy between the calculated and observed transitions to the ground state.

The ^{90}Zr proton strength function determined from this work is shown in Fig. 9. Along with the total strength function, there is shown the contribution from each significant decay channel. Apparent in this is the strong competition between the radiative capture and compound elastic scattering channels at low proton energy and between compound elastic and inelastic scattering at high energy. Previous studies[1–7] of proton strength functions in this mass region using proton elastic and neutron channels have not shown these strong competition effects, since the neutron channel usually dominates in the decay of the compound nucleus, for energies above the (p,n) threshold. As observed in previous (p,n) studies[5] of ^{92}Zr and ^{94}Zr the strength function shows a valley near 4 MeV due to the $3s$ SPR and a rise toward higher energy to the $3p$ SPR.

The small values of the absorptive potential strength and the real diffuseness for ^{90}Zr obtained from the analysis of the proton absorption data are consistent with previous results for ^{92}Zr and ^{94}Zr,[5] showing a trend of decreasing values near the closed neutron shell at $N=50$.

ACKNOWLEDGMENTS

APPENDIX: THE NUCLEON-NUCLEUS INTERACTION MODEL—LANE MODEL

The nuclear optical model with a complex potential as suggested by Lane[20] [of the form $v=v_0+v_1(\tau\cdot\mathbf{T})/A$] is the basis for the analysis of the proton absorption and scattering in ^{90}Zr as given here. For protons interacting with a nucleus of isospin $T=T_0=(N-Z)/2$, the Schrödinger equation with real potentials (V,W) reduces to the coupled equations (see Refs. 18, 6, and 26)

$$(\tau+V_{\mathrm{p}}+iW_{\mathrm{p}}+V_C-E)g_{\mathrm{p}}=Bg_{\mathrm{n}} \tag{A1}$$

and

$$(\tau+V_{\mathrm{n}}+iW_{\mathrm{n}}+\Delta_C-E)g_{\mathrm{n}}=Bg_{\mathrm{n}} , \tag{A1'}$$

where

$$B=v_1\sqrt{T_0/2}/A , \tag{A2}$$

$$V_{\mathrm{p}}=\mathrm{Re}(v_0-v_1T_0/2A) , \tag{A3}$$

$$V_{\mathrm{n}}=\mathrm{Re}[v_0+v_1(T_0-1)/2A] , \tag{A4}$$

$$W_{\mathrm{p}}=\mathrm{Im}(v_0-v_1T_0/2A) , \tag{A5}$$

$$W_{\mathrm{n}}=\mathrm{Im}[v_0+v_1(T_0-1)/2A] , \tag{A6}$$

and $i=\sqrt{-1}$. Both real and imaginary potentials are in general functions of r and E. The proton kinetic energy is represented by the operator τ and E is the proton energy, while the spatial wave functions g_{p} and g_{n} represent amplitudes for finding the system in the configuration consisting of a proton plus the target and a neutron plus analog of the target, respectively. The Coulomb potential V_C is that of a uniform spherical charge distribution with $R_C=1.23A^{1/3}$ fm. The charge radius R_C yields an rms radius consistent with that deduced from electron scattering experiments.[31]

If B is set equal to zero in Eqs. (A1) and (A1'), or if the off-diagonal terms of $\tau\cdot\mathbf{T}$ are neglected, while keeping v_1 nonzero (clearly inconsistent with the Lane model), then the conventional optical model with asymmetry terms is obtained from $v_1T_0/2A=v_1(N-Z)/4A$ for both the real, V_{p}, and absorptive W_{p}, potentials.

In the present work, the real part of the proton optical potential is given by

$$V_P(r,E)=-V_R(E)f(X_R)+V_{\mathrm{so}}\frac{df}{dr}(X_{\mathrm{so}})\mathbf{l}\cdot\mathbf{s}/r-V_C(R_C) , \tag{A7}$$

where

$$V_R(E)=V_0-\beta E+V_1(N-Z)/A+V_C(R_C) \tag{A8}$$

and

$$f(X_j)=1/[1+\exp(X_j)] , \tag{A9}$$

$$X_j=(r-R_jA^{1/3})/a_j , $$

and $j=R$, so, or D.

The absorptive potential W_{p} is given by

$$W_{\mathrm{p}}=4W_Ddf(X_D)/dr . \tag{A10}$$

The unique determination of the potentials in both channels requires additional information obtained by examining the neutron-nucleus interaction. The Lane potential $v_0 + v_1(\tau \cdot T_0/A)$ applied to a neutron interaction with a nucleus gives the Schrödinger equation

$$(\tau + V_{nc} + iW_{nc} + \Delta_C - E)g_{nc} = 0 , \qquad \text{(A11)}$$

where

$$V_{nc} = \mathrm{Re}(v_0 + v_1 T_0/2A) , \qquad \text{(A12)}$$

$$W_{nc} = \mathrm{Im}(v_0 + v_1 T_0/2A) , \qquad \text{(A13)}$$

and nc refers to the neutron plus core interaction. Since the energies of interest in the present work are less than the Coulomb energy Δ_C, Eq. (A11) describes low-lying bound "parent states" in ^{91}Zr. For such a system, it was assumed that the imaginary part of the neutron-nucleus interaction, W_{nc}, was zero.[29] This assumption leads to the constraint that W_n, in Eq. (A8), is given by

$$W_n = \mathrm{Im}(-v_1/2A) ,$$

and more importantly that

$$W_n = W_p/2T_0 .$$

*Present address: Nichols Research Corporation, 4040 South Memorial Parkway, Huntsville AL 35805.

[1]C. H. Johnson, J. K. Bair, C. M. Jones, S. K. Penny, and D. W. Smith, Phys. Rev. C **15**, 196 (1977).

[2]C. H. Johnson, A. Galonsky, and R. L, Kernell, Phys. Rev. Lett. **39**, 1604 (1977); Phys. Rev. C **20**, 2052 (1979).

[3]D. S. Flynn, R. L. Hershberger, and F. Gabbard, Phys. Rev. C **20**, 1700 (1979).

[4]R. Schrils, D. S. Flynn, R. L. Hershberger, and F. Gabbard, Phys. Rev. C **20**, 1706 (1979).

[5]D. S. Flynn, R. L. Hershberger, and F. Gabbard, Phys. Rev. C **31**, 87 (1985).

[6]D. S. Flynn, R. L. Hershberger, and F. Gabbard, Phys. Rev. C **26**, 1744 (1982).

[7]R. L. Hershberger, D. S. Flynn, F. Gabbard, and C. H. Johnson, Phys. Rev. C **21**, 896 (1980).

[8]A. B. Smith, P. T. Guenther, and J. F. Whalen, Nucl. Phys. **A415**, 1 (1984).

[9]*Tables of Isotopes*, 7th ed., edited by C. M. Lederer and Virginia S. Shirley (Wiley, New York, 1978).

[10]A. Antilla, J. Keinonen, M. Hautala, and I. Forsblom, Nucl. Instrum. Methods **147**, 501 (1977).

[11]M. J. Kenny, J. R. Bird, and E. Clayton, Nucl. Instrum. Methods **168**, 115 (1980).

[12]See AIP document No. PAPS PRVCA-35-1265-1 for 1 page of ^{90}Zr(p,p) cross sections. Order by PAPS number and journal reference from American Institute of Physics, Physics Auxiliary Publications Service, 335 East 45th Street, New York, NY 10017. The price is $1.50 for each microfiche (98 pages) or $5.00 for photocopies of up to 30 pages, and $0.15 for each additional page over 30 pages. Airmail additional. Make checks payable to the American Institute of Physics.

[13]J. T. Routti and S. G. Prussian, Nucl. Instrum. Methods **72**, 125 (1969).

[14]H. Weidenmüller, Nucl. Data Sheets **31**, 181 (1980).

[15]F. Rauch, Z. Phys. **243**, 105 (1971).

[16]C. F. Moore, S. A. A. Zaidi, and J. J. Kent, Phys. Rev. Lett. **18**, 345 (1967).

[17]C. H. Johnson, Phys. Rev. C **16**, 2238 (1977).

[18]P. G. Young and E. D. Arthur, Los Alamos Scientific Laboratory Report LA-6947, 1977.

[19]W. Hauser and H. Feshbach, Phys. Rev. **87**, 366 (1952).

[20]A. M. Lane, Nucl. Phys. **35**, 676 (1962).

[21]A. H. Wapstra and K. Bos, At. Data Nucl. Data Tables **19**, 215 (1977).

[22]W. Dilg, W. Schantl, H. Vonach, and M. Uhl, Nucl. Phys. **A127**, 269 (1973).

[23]D. E. Hodgson, *Nuclear Reactions and Nuclear Structure* (Clarendon, Oxford, 1971), p. 290; L. Dresner, in Proceedings of the International Conference on the Neutron Interaction with the Nucleus, Columbia University, New York, 1957, United States Atomic Energy Commission Report USAEC TIC-7547, 1957, p. 71.

[24]W. S. Courtney and J. D. Fox, At. Data Nucl. Data Tables **15**, 141 (1975).

[25]F. D. Becchetti, Jr., and G. W. Greenless, Phys. Rev. **182**, 1190 (1969).

[26]D. S. Flynn, Phys. Rev. C **27**, 2381 (1983).

[27]G. Vourvopoulos, R. Shoup, J. D. Fox, and J. B. Ball, in *Nuclear Isospin*, edited by J. D. Anderson, S. D. Bloom, J. Cerny, and W. W. True (Academic, New York, 1969), p. 205.

[28]K. L. Knöpfle, M. Rogge, C. Meyer-Boricke, J. Pedersen, and D. Burch, Nucl. Phys. **A159**, 642 (1970).

[29]E. H. Auerbach, C. B. Dover, A. K. Kerman, R. H. Lemmer, and E. H. Schwartz, Phys. Rev. Lett. **17**, 1184 (1966); G. C. Dutt and R. Schrils, Phys. Rev. **175**, 1413 (1968).

[30]S. M. Grimes, Phys. Rev. C **22**, 436 (1980).

[31]K. Schulte, G. Berg, P. von Brentano, and H. Paetz gen. Schieck, Nucl. Phys. **A241**, 272 (1975).

[32]F. G. Perey, Phys. Rev. **131**, 745 (1963).

[33]S. L. Tabor, B. A. Watson, and S. S. Hanna, Phys. Rev. C **11**, 198 (1975).

[34]G. W. Greenlees, G. J. Pyle, and Y. C. Tang, Phys. Rev. **171**, 1115 (1968).

[35]R. C. Barrett and D. F. Jackson, *Nuclear Sizes and Structure* (Clarendon, Oxford, 1977), pp. 142–185.

[36]L. A. Fajardo, J. R. Ficenec, W. P. Trower, and I. Sick, Phys. Lett. **37B**, 363 (1971).

[37]H. Beil, R. Bergerè, P. Carlos, A. Leprêtre, A. DeMiniac, and A. Veyssiére, Nucl. Phys. **A227**, 427 (1974).

[38]D. Brajnik, D. Jamnik, G. Kernel, M. Korun, U. Miklavžič, B. Pucelj, and A. Stanovnik, Phys. Rev. C **13**, 1852 (1976).

[39]A. Leperêtre, H. Beil, R. Bergère, P. Carlos, A. Veyssiére, and M. Sugawara, Nucl. Phys. **A175**, 609 (1971).

[40]G. A. Bartholomew, E. D. Earle, A. J. Ferguson, J. W. Knowles, and M. A. Lone, Adv. Nucl. Phys. **7**, 229 (1973).

[41]E. Obst, F. Rauch, and E. Rössler, Phys. Lett. **21**, 50 (1966).

[42]K. Nilson, B. Erlandsson, and A. Marcinkowski, Nucl. Phys. **A391**, 61 (1982), and references therein.

[43]S. J. Burger and G. Heymann, Nucl. Phys. **A243**, 461 (1975).